

Discovery of an active supermassive black hole in the bulge-less galaxy NGC 4561.

C. Araya Salvo¹, S. Mathur¹, H. Ghosh², F. Fiore³, L. Ferrarese⁴

ABSTRACT

We present *XMM-Newton* observations of the *Chandra*-detected nuclear X-ray source in NGC 4561. The hard X-ray spectrum can be described by a model composed of an absorbed power-law with $\Gamma = 2.5_{-0.3}^{+0.4}$, and column density $N_H = 1.9_{-0.2}^{+0.1} \times 10^{22}$ atoms cm^{-2} . The absorption corrected luminosity of the source is $L(0.2 - 10.0 \text{ keV}) = 2.5 \times 10^{41}$ ergs s^{-1} , with bolometric luminosity over 3×10^{42} ergs s^{-1} . Based on the spectrum and the luminosity, we identify the nuclear X-ray source in NGC 4561 to be an AGN, with a black hole of mass $M_{\text{BH}} > 2 \times 10^4 M_{\odot}$. The presence of a supermassive black hole at the center of this bulge-less galaxy shows that black hole masses are not necessarily related to bulge properties, contrary to the general belief. Observations such as these call into question several theoretical models of BH-galaxy co-evolution that are based on merger-driven BH growth; secular processes clearly play an important role. Several emission lines are detected in the soft X-ray spectrum of the source which can be well parametrized by an absorbed diffuse thermal plasma with non-solar abundances of some heavy elements. Similar soft X-ray emission is observed in spectra of Seyfert 2 galaxies and low luminosity AGNs, suggesting an origin in the circumnuclear plasma.

Subject headings: galaxies: active — galaxies: individual (NGC 4561) — galaxies: nuclei — X-rays: individual (NGC 4561)

¹Department of Astronomy, The Ohio State University, 140 W 18th Ave, Columbus, OH 43210; araya@astronomy.ohio-state.edu

²CNRS/CEA-Saclay, 91911 Gif-sur-Yvette, France

³Osservatorio Astronomico di Roma, via Frascati 33, 100040 Monteporzio Catone, Italy

⁴Hertzberg Institute of Astrophysics, 5071 West Saanich Road, Victoria, BC, V9E 2E7, Canada

1. INTRODUCTION

The past decade has seen extraordinary growth in our understanding of supermassive black holes (SMBHs), with secure detections, mass measurements and new demographic information (see Ferrarese & Ford 2005 and references therein). Knowledge of the mass function of SMBHs directly affects our understanding of SMBH formation and growth, nuclear activity, and the relation of SMBHs to the formation and evolution of galaxies in hierarchical cold dark matter models (e.g., Menci et al. 2004). The cumulative mass function needed to explain the energetics of high redshift quasars implies that all galaxies in the local universe should host a SMBH (e.g., Marconi et al. 2004, Shankar et al. 2004).

Observationally, however, we do not know whether every galaxy hosts a SMBH. Traditional methods of finding SMBHs, viz. stellar dynamics and gas dynamics are powerful only at the high-mass end of the SMBH mass function: the BH sphere of influence cannot be resolved for BH masses less than $10^6 M_{\odot}$ beyond a distance of a couple of Mpc, even with *HST* (Ferrarese & Ford 2005). One way, and perhaps the most efficient way to find SMBHs in galaxies is to look for active SMBHs. In fact, looking for AGN activity is perhaps the only viable way to probe the low-mass end of the local SMBH mass function. X-ray observations provide the best opportunity for this purpose because X-ray emission is an ubiquitous property of AGNs and X-rays can penetrate obscuring material that might hide an AGN at other wavelengths. Indeed, X-ray observations have detected AGN activity in what were thought to be “normal” galaxies in clusters (e.g., Martini et al. 2002) and in the field (e.g., Brand et al. 2005).

In an effort to study the demographics of local SMBHs, we had undertaken a *Chandra* program to look for nuclear X-ray sources in nearby optically “normal” spiral galaxies (within 20Mpc). This program was highly successful; we discovered AGNs in the nuclei of what were thought to be “normal” galaxies (Ghosh et al. 2008, Ghosh 2009, Ghosh et al. 2011; see also Zhang et al. 2009; Desroches & Ho 2009). The nuclear X-ray sources, however, could be stars, binaries, supernova remnants or AGNs. Through extensive spectral, timing, and multiwavelength analysis we classified the nuclear X-ray sources and found 17 (out of 56 surveyed) that are almost certainly low-luminosity AGNs. Thus at least 30% of “normal” galaxies are actually active. The inferred luminosities of these sources range from $10^{37.5}$ to 10^{42} ergs s^{-1} . In a few objects where SMBH masses were known from stellar/gas velocity dispersion methods, we find accretion rates as low as 10^{-5} of the Eddington limit, comparable to what has been found in LINERS (e.g., Dudik et al. 2005).

We then expanded upon the initial *Chandra* survey by using the sample of SINGS galaxies (Spitzer INfrared Galaxy Survey; Kennicutt et al. 2003). Out of the 75 SINGS galaxies, 60 have data in the *Chandra* archive and we detected nuclear X-ray sources in 36

of them (Grier et al. 2011). This once again shows that X-ray observations are far more efficient at detecting AGNs than optical.

As noted above, through multiwavelength analysis we have shown that a large fraction of the *Chandra*-detected nuclear X-ray sources are indeed AGNs. Additionally, using statistical arguments we have shown most of them to be AGNs (Ghosh et al. 2010, Grier et al. 2011). We obtained *XMM-Newton* spectra of several of our *Chandra*-detected nuclear X-ray sources with the goal of obtaining secure identifications as either AGNs or other contaminants. In this paper we focus on the bulge-less galaxy NGC 4561 for the following reason.

The mass of the supermassive black holes (BHs) in centers of galaxies was found to be correlated with the bulge luminosity of host galaxies ($M_{\text{BH}} - L_{\text{Bulge}}$ relation; Magorrian et al. 1998; revised in Gültekin et al. 2009). Even a tighter correlation was later found between the BH mass and the velocity dispersion (σ) of the bulge ($M_{\text{BH}} - \sigma$ relation; Gebhardt et al. 2000, Ferrarese & Merritt 2000, Merritt & Ferrarese 2001). Basically, the mass of the black hole seems to be correlated with the mass of the bulge (Häring & Rix 2004). The above relations for normal galaxies also extend to active galaxies (e.g., McLure & Dunlop 2002, Woo & Urry 2002). These results were interpreted to imply that the formation and growth of the nuclear black hole and the bulge in a galaxy are intimately related, and several theoretical models have attempted to explain the observed $M_{\text{BH}} - \sigma$ and $M_{\text{BH}} - L_{\text{Bulge}}$ relations (e.g. Adams et al. 2001, Di Matteo et al. 2003). The hydrodynamic cosmological simulations, such as those of Hopkins et al. 2006, naturally account for BH–galaxy co-evolution. In all such models, the bulge determines the nuclear BH mass. In the models of Volonteri and Natarajan (2009) seed BH masses are correlated to the host dark matter properties; these seeds could have been formed by direct collapse of pre-galactic halos (Begelman et al. 2006). Major mergers then trigger simultaneous BH growth and star formation resulting in a tight coupling between the two. A clear prediction of these models is that low-mass bulge-less galaxies today are unlikely to host nuclear BHs (Volonteri, Natarajan & Gültekin 2011). Finding AGNs in bulge-less galaxies would certainly be a challenge for such models. Perhaps the BHs in bulge-less galaxies represent the seed BHs that have not yet grown. It has also been shown that the merger and SMBH growing process may not create a bulge because of star formation and, mainly, because of supernova feedback (Governato et al. 2010). Recent studies have shown that even moderate-luminosity AGNs up to $z \sim 3$ are powered mostly through internally driven processes (Mullaney et al. 2011), and that mergers do not play a major role in triggering AGNs (Cisternas et al. 2011, Schawinski et al. 2011). Thus the role of mergers in the growth of SMBHs remains a matter of debate and SMBHs in bulge-less galaxies provide an important piece of the puzzle. Enlarging the sample of these objects is thus crucial to learn their properties and to be able to understand their formation and evolution mechanisms.

In this paper we present *XMM-Newton* data of the nuclear X-ray source in the bulge-less galaxy NGC 4561 which shows evidence of being an AGN. This secure identification of a SMBH in a bulge-less galaxy shows that a bulge is not necessary for the existence of a BH and the presence of SMBHs in bulge-less galaxies is more common than expected.

2. NGC 4561

NGC 4561 (Sdm) is a late-type bulge-less spiral galaxy at $z=0.00469$. It follows the selection criteria used in our previous *Chandra* survey (close to face on with inclination less than 35° to ensure that the nuclear source is not obscured by the disk of the host galaxy; Galactic latitude $|b| > 30^\circ$ to avoid obscuration and contamination from our own galaxy; and no known starburst or AGN activity) in which a nuclear X-ray source was detected (Ghosh 2009). The optical spectra of NGC 4561 were analyzed by Kirhakos & Steiner 1990, who classified it as an H II region-like galaxy.

The nuclear X-ray source was detected in a *Chandra* observation with 103 net counts with a count rate of 0.029 ± 0.003 ct/s. The source was found to be hard ($HR = -0.53^{+0.14}_{-0.13}$). The spectrum was fitted with a power law $\Gamma = 1.5 \pm 0.3$ and no intrinsic absorption ($N_H \leq 1.7 \times 10^{21}$ cm $^{-2}$). With this model the flux was $F(0.3 - 8 \text{ keV}) = 2.5 \times 10^{-13}$ ergs cm $^{-2}$ s $^{-1}$ which corresponds to a luminosity of $L(0.3 - 8 \text{ keV}) \simeq 5 \times 10^{39}$ ergs s $^{-1}$. This luminosity is a lower limit: the hardness of the source indicates that the source is likely to be absorbed. The quality of the *Chandra* data, however, was not good enough to determine the spectral shape accurately. The hardness of the emission and the high enough luminosity make this source a good candidate AGN (Ghosh 2009).

The *Chandra* observations also showed a second source at $7''$ from the nucleus (source “B” here onward), which is soft ($HR = -0.9$) and its flux is only 10% of the nuclear source flux. Even though source B won’t be resolved by *XMM-Newton*, its effect on the spectrum of the nuclear X-ray source should be minimal.

3. Observations and Data Reduction

Our target was observed with *XMM-Newton* on the 2009 July 10. For the European Photon Imaging Camera (EPIC), the exposure times were 57022 s for MOS1, 57038 s for MOS2 and 55960 s for pn; all of these exposures were obtained using the thin filter in extended full frame.

The data were processed and filtered using SAS v9.0.0 using tasks *epchain* and *emchain*.

Before the source extraction, we applied standard and temporal filters to the event list. For the standard filter we selected the energy to be between 0.2 and 15 keV for pn and between 0.2 and 12 keV for MOS, single or double pixel events (`PATTERN <= 4`) for pn and single, double or triple pixel events for MOS (`PATTERN <= 12`), with good flag values (`#XMMEA_EP`) for pn and (`#XMMEA_EM`) for MOS. For the temporal filters we created light curves for the 10-12 keV band selecting only events with `PATTERN==0` (as recommended at the XMM SAS User Guide)¹. The good time intervals were created by rejecting the intervals with count rates higher than 0.5 cts/s for pn and 0.25 cts/s for MOS. The effective exposure time is 26.3 ks (for pn) corresponding to 47% of the observation time. The effective exposure times for MOS after applying the GTI are 36.7ks (64%) for MOS1 and 37.6ks (66%) for MOS2.

Within the circular extraction region of 20" radius the total number of counts detected in the PN data was 6638 cts with a rate of 0.282 ± 0.004 cts s⁻¹. The exposure time at the source (after vignetting correction) was 21.91 ks. Our source was detected in soft and hard X-rays with 4529.4 cts (0.2-2.5 keV) and 1581.7 cts (2.5-10.0 keV), which corresponds to $HR = -0.48 \pm 0.01$. The background level was of 2.13 cts/pixel. There were no considerable variations on the count rate during the observation.

3.1. The spectra

For extracting the spectrum we used a selection area of a 20" radius circle centered at the source and selected only events with `FLAG==0` in order to obtain a good quality spectrum. When extracting the background spectrum we used a square of 41" side. Finally the RMF and ARF files were created and *backscale* was ran. Corrections for Out of time (OoT) events or Pile up were not needed.

The spectrum was analyzed using Xspec v12.6.0 (HEASOFT). We binned the spectra using *grppha* with a minimum of 50 cts per bin for the PN spectrum and 40 cts per bin for the MOS1 and MOS2 spectra.

3.1.1. Checking for possible contamination

We checked if spectrum was contaminated. This was a possibility given that there is a third source at 32" from the nucleus (source C here onward), which could contaminate the

¹http://xmm.esa.int/external/xmm_user_support/documentation/sas_usg/USG/

source spectrum. The source extraction radius of 26.65” encircles 90% of the energy, so some contamination from source C is expected. In order to see how important this contamination was, we tried different selection areas when extracting the spectrum: (1) a circle with a radius of 20” centered at the source; (2) a circle with a radius of 26.65” (which encircles 90% of the total energy); (3) the same 26.65” circle but excluding a 26.65” circle around source C; and (4) a 26.65” radius semicircle on the opposite side of the source C.

These selection areas are shown in figure 1. Emission line-like features were present in all of the 4 extracted spectra, discussed further in §4. Also, all of the spectra have similar values for Γ and for the observed flux showing that the contamination is negligible, and that the emission features present in the spectrum are real.

3.1.2. The fitting process

The spectral fitting was performed on the PN spectrum for energies $E \geq 0.3$ keV. Because of the considerably lower signal to noise of the MOS data, it did not help to constrain the parameters any better. Once the final models were chosen, we tried them on the MOS1 and MOS2 spectrum and confirmed that they are consistent.

To fit the spectra, different models were tried, always with a fixed galactic absorption of $N_H = 2.11 \times 10^{20} \text{ cm}^{-2}$ and a free intrinsic absorption. Both absorption components were represented with the “wabs” model for photoelectric absorption.

First we tried with a power law, which by itself does not provide a good fit ($\chi^2_\nu = 1.28$ for 114 dof) and overestimates the counts for high energies. To avoid the latter issue we fitted the absorbed power law using only the hard part of the spectra ($E \geq 2.5$ keV). To get a good fit in the hard range of energies, intrinsic absorption is needed (as suspected from the *Chandra* observation). We needed another component to model the soft-band, since the power law is almost completely absorbed in the soft-band (see figure 2). The resulting photon index was $\Gamma = 2.46$. From here on, when fitting the spectrum over the entire energy range, the Γ parameter was kept frozen at this value. In order to characterize the unresolved nearby source (source B), we also added a black body component with a flux of $F(0.3-8\text{keV}) = 2.5 \times 10^{-14} \text{ ergs cm}^{-2} \text{ s}^{-1}$ corresponding to the flux observed with *Chandra* and a temperature of $kT = 0.2$ keV. Both the temperature and the normalization were always fixed.

Since the hard-band is well fit by a power-law, our next task is to fit the soft component with different models. Because the spectrum shows “emission-like” features, we tried an absorbed “mekal” model, which characterizes emission from hot diffuse gas, but the fit was

not good ($\chi^2_{\nu}=2.35$ for 112 dof, even worse than the absorbed power law with $\Delta\chi^2 = -117.3$, figure 3). This fit was done fixing the abundance to the Solar value. Leaving this parameter free does not improve the fit considerably ($\chi^2_{\nu}=2.27$ for 111 dof, figure 4).

We also tried to fit the soft component with the “vmekal” model, same as “mekal” but allows the abundances of each element to vary individually. A good fit was finally found using vmekal when leaving the abundances of some of the heavier elements as free parameters. This model has $\chi^2_{\nu}=1.11$ for 107 dof (figure 5), that corresponds to $\Delta\chi^2 = 144.43$ when compared to the fit with solar abundances.

It is possible that in the soft-band we are observing the continuum reflected off some nearby scattering material. For this reason, we also tried the “reflionx” model (reflection by a constant density illuminated atmosphere). This model does reproduce some emission lines, but the fit is not good and it is also a worse fit than the absorbed power law ($\chi^2_{\nu}=1.39$ for 113 dof, $\Delta\chi^2 = -11.18$ when compared to the absorbed power law model, figure 6).

4. Results

The best fitted model is composed of an absorbed power law with $\Gamma = 2.5^{+0.4}_{-0.3}$ and $N_H = 2.0^{+0.3}_{-0.2} \times 10^{22} \text{ cm}^{-2}$ and an absorbed thermal plasma component with non-solar abundances for some of the heavy elements (O = $0.33^{+0.14}_{-0.12}$, Na = 34^{+11}_{-8} , Si ≤ 0.2 , Fe = $0.12^{+0.06}_{-0.04}$, Ni ≤ 0.4) with a temperature of $kT = 0.59^{+0.04}_{-0.05} \text{ keV}$ and $N_H = 7^{+2}_{-4} \times 10^{20} \text{ cm}^{-2}$ (and a black body for the source B). The fit to the spectrum is presented in figure 5 and the corresponding theoretical model in figure 7. The observed flux is $F(0.2 - 10 \text{ keV}) = 1.2 \times 10^{-12} \text{ ergs cm}^{-2} \text{ s}^{-1}$ which corresponds to a luminosity of $L(0.2 - 10.0 \text{ keV}) = 5.8 \times 10^{40} \text{ ergs s}^{-1}$. The unabsorbed luminosity is $L(0.2 - 10.0 \text{ keV}) = 2.5 \times 10^{41} \text{ ergs s}^{-1}$. The bolometric luminosity of the source is therefore about $3.5 \times 10^{42} \text{ ergs s}^{-1}$ (assuming a bolometric correction factor of 14 for this luminosity; Vasudevan & Fabian 2007), putting it squarely in the luminosity range observed for AGNs.

5. Discussion

The hard-band spectrum of the nuclear X-ray source in NGC 4561 can be described as a power law with photon index $\Gamma = 2.5^{+0.4}_{-0.3}$. Most of the soft component of the power law is absorbed (intrinsic absorption of $N_H = 2.0^{+0.3}_{-0.2} \times 10^{22} \text{ cm}^{-2}$). The source shows a hardness ratio of $HR = -0.48 \pm 0.01$ and an absorption corrected luminosity of $L(0.2 - 10.0 \text{ keV}) = 2.5 \times 10^{41} \text{ ergs s}^{-1}$. The photon index and the high luminosity of the source are indications

of the presence of an active SMBH in the center of NGC 4561.

The soft emission can be modeled as an absorbed thermal plasma with $kT = 0.59_{-0.05}^{+0.04}$ keV and non-solar abundances as follow: $O = 0.33_{-0.12}^{+0.14}$, $Na = 34_{-8}^{+11}$, $Si \leq 0.2$, $Fe = 0.12_{-0.04}^{+0.06}$ and $Ni \leq 0.4$, with 1.0 corresponding to the Solar values.

No other model was capable of providing a good fit for the spectrum. It is quite interesting that non-solar abundances are needed for some elements. The nickel abundance is consistent with the solar value within the 3σ contour. For oxygen, sodium, silicon and iron the abundances are not consistent with the solar values as can be seen in the contour plots (figures 8, 9, 10 and 11 for O, Na, Si and Fe respectively), they are sub-solar for oxygen, silicon and iron but super-solar for sodium. It is important to note that when these parameters are kept frozen at solar value the model does not provide a good fit. Different abundances for different elements suggest that the observed thermal plasma is not well mixed in heavy elements or that the models we use are too simplistic to describe its physical conditions.

Abundances for some elements in AGNs have been measured before, for example in Mrk 1044 and Mrk 279, where super-solar abundances for C, Ni, O and Fe were found (Fields et al. 2005, Fields et al. 2007). Hamann & Ferland 1999 find that high-redshift quasars also have super-solar metallicities. Later studies showed that quasars have super-solar abundances at all redshifts (Hamann & Simon 2010) which would be consistent with the scenario of AGNs appearing after an important star formation event. Sub-solar abundances, however, have been observed in the vicinity of AGNs like in the spectrum of NGC 1365 (Guainazzi et al. 2009), that shows sub-solar abundances of carbon, nitrogen, oxygen, neon, magnesium, silicon and iron. Sub-solar abundances were inferred also for the sample of LLAGNs, LINERs and starburst galaxies presented in Ptak et al. 1999.

The temperature for the thermal plasma, $kT = 0.59_{-0.05}^{+0.04}$ keV, is similar to what has been found in similar objects like NGC 3367 and NGC 4536 ($kT = 0.64 \pm 0.03$ keV and $kT = 0.58 \pm 0.03$ keV respectively, McAlpine et al. 2011), and in agreement with what is expected for LLAGNs; $kT \approx 0.4 - 0.8$ keV (Ho 2008).

Levenson et al. 2001 have analyzed ROSAT and ASCA data of Seyfert 2 galaxies with starbursts; they found that most of the soft emission, which is modeled with a thermal component, is produced by star formation. The median temperature of this component for their sample is about 0.6–0.7 keV. In their analysis, solar abundances were used because the quality of the data would not allow a measure of metallicity, but they do mention that low abundances are required in high-resolution spectra of starburst galaxies as shown by Dahlem et al. 1998. Given the similarity of the temperature of the thermal component and the sub-solar abundances of NGC 4561 that we find, the soft X-ray emission we observe

could be produced by nuclear star formation.

No variability was observed during the observation but there was a variation between the *Chandra* observation on 2006 March 15 and our *XMM-Newton* observation. From the count rate observed on *Chandra* (0.029 cts/s), PIMMS predicts a count rate of 0.072 cts/s for XMM PN using the thin filter and the whole PSF (~ 5 arcmin). We expect a more realistic value of about 78% of this rate, given the smaller (20" radius) PSF we used; it corresponds to 0.056 cts/s. Our observed count rate of 0.282 ± 0.004 cts/s is 5 times higher than expected. This variation might have resulted from the change in the absorber column density. The variability also supports the AGN scenario.

A lower limit on the black hole mass can be obtained assuming the black hole radiates at Eddington luminosity; for $L_{\text{bol}} = 3 \times 10^{42}$ ergs s^{-1} , the BH must have a mass $M_{\text{BH}} > 2 \times 10^4 M_{\odot}$. This is an exciting discovery of a SMBH in a bulge-less galaxy. To our knowledge, two bulge-less galaxies are known to host AGNs from optical studies: NGC 4395 (Sdm; Filippenko & Sargent 1989, Peterson et al. 2005) and NGC 1042 (Scd; Shields et al. 2008). Both galaxies host a nuclear star cluster. IR spectroscopy with *Spitzer* led to the discovery of AGNs in two more Sd galaxies, NGC 3621 (Satyapal et al. 2007) and NGC 4178 (Satyapal et al. 2009). These two also harbor a nuclear star cluster. Using *XMM-Newton*, 2 other AGNs in bulge-less galaxies have been confirmed by McAlpine et al. 2011: one in NGC 3367 (Sc) and the other in NGC 4536 (SABbc). We found nuclear X-ray sources in M101 (type Scd), NGC 4713 (Sd), NGC 3184 (Scd), and NGC 4561 (Sdm) (Ghosh et al. 2008, Ghosh 2009, Ghosh et al. 2011) and argued that they are likely to be AGNs. The dwarf starburst galaxy Henize 2-10 is very likely to host an AGN too (Reines et al. 2011). In this paper we present conclusive evidence that NGC 4561 does in fact host an AGN. The discovery of SMBHs in the nuclei of these galaxies calls into question whether the masses of SMBHs are governed by bulge properties (§1). These results suggest that SMBH in bulge-less galaxies are far more common than what we previously thought, in clear disagreement with some models of BH growth. A key prediction of the models of Volonteri & Natarajan (2009) is that low-mass bulge-less galaxies today are unlikely to host nuclear black holes, which does not seem to be the case. While BHs grow through merger-driven processes, alternative tracks of BH growth must exist; secular process appear to play an important role.

About 75% of late-type galaxies host nuclear star-clusters (Böker et al. 2004). Is the SMBH related to the mass of the star-cluster then (Seth et al. 2008)? Or is it the dark matter halo (Baes et al. 2003)? Are the BHs in bulge-less galaxies the seed BHs at high redshift that did not grow? Answering these kind of questions is fundamental to our knowledge of BH–galaxy formation and co-evolution.

6. Conclusions

We present *XMM-Newton* spectrum of the *Chandra*-detected nuclear source in NGC 4561 and show that it is an obscured AGN. The existence of nuclear SMBHs in bulge-less galaxies shows that BH masses are not governed by bulge properties. This calls into question several theoretical models (§1) of BH–galaxy co-evolution which are merger-driven; secular processes clearly play an important role in BH growth.

Acknowledgment: We gratefully acknowledge support from the NASA grant NNX09AP85G to SM.

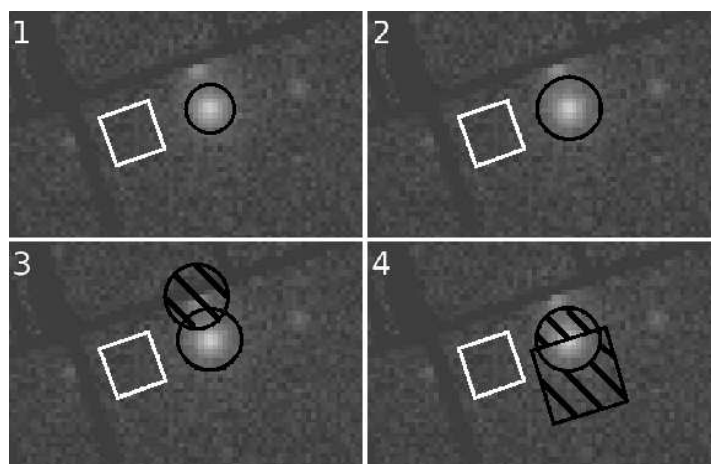


Fig. 1.— The EPIC-pn image of the source; the four panels show the different areas used to extract the spectrum when checking for possible contamination. To select the background spectrum the same $41''$ side square (in white) was used all the time. The different selection areas (in black) for the spectrum are: (1) $20''$ radius circle, (2) $26.65''$ radius circle, (3) $26.65''$ circle radius excluding a circle of the same size around the closest source and (4) a $26.65''$ radius semicircle opposite to the closest source.

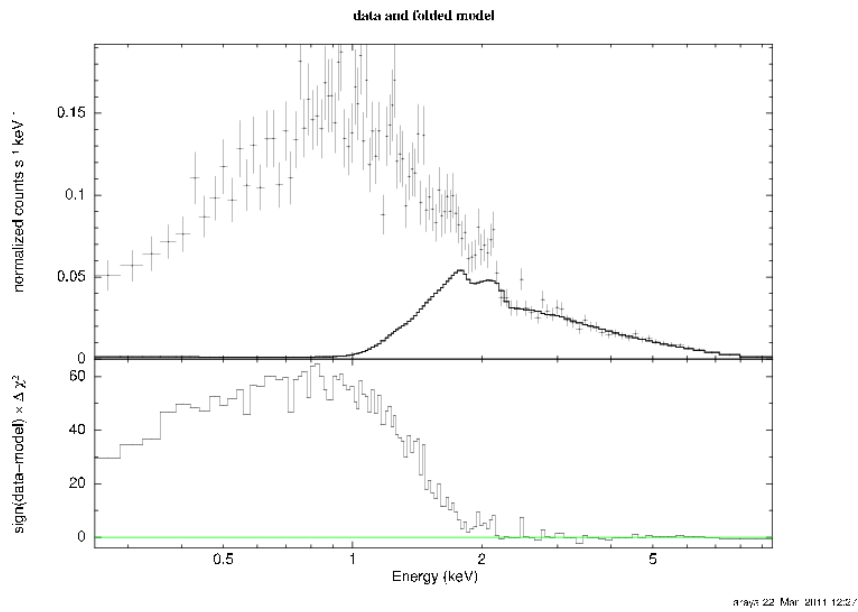


Fig. 2.— The extracted spectrum and the model of an absorbed power law fitted to $E > 2.5$ keV. The bottom panel shows the contributions to χ^2 after extrapolating the model to the entire energy range. Significant absorption is needed to fit the hard end of the spectrum properly.

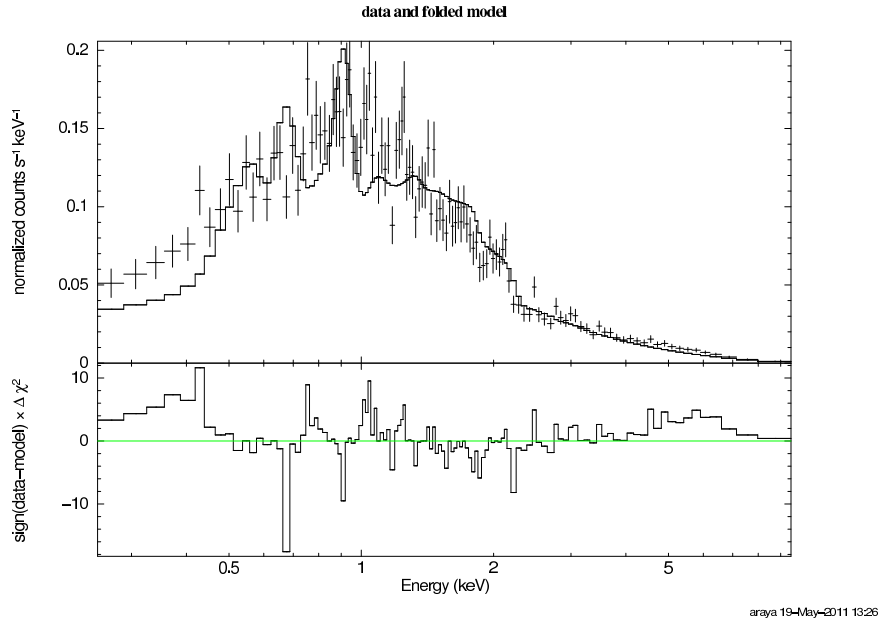


Fig. 3.— The data fitted with an absorbed power-law plus the diffuse thermal plasma model (“mekal”) with solar abundances and a black body. Contributions to χ^2 are presented in the bottom panel and show that this model does not fit the data well.

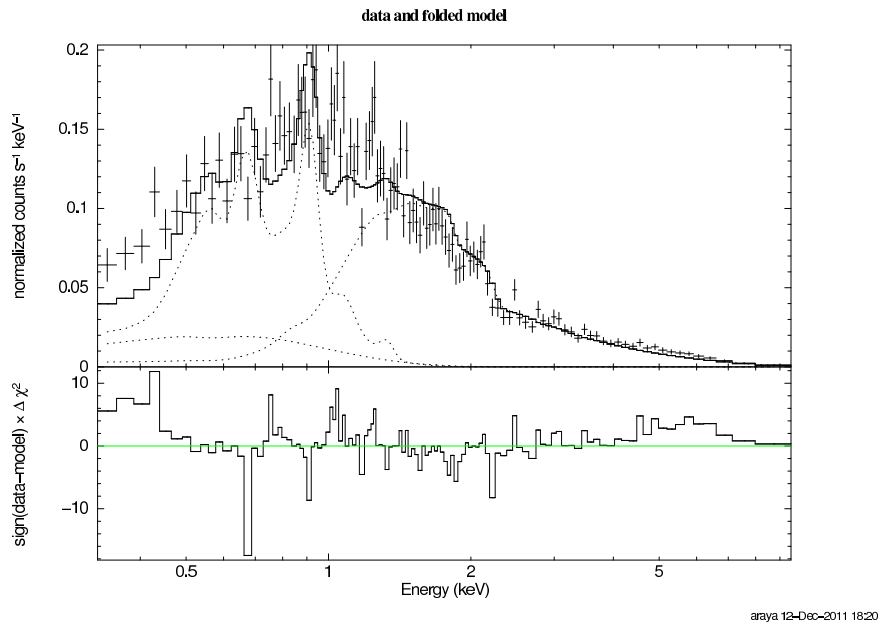


Fig. 4.— Same as Fig. 3, but with a constant non-solar abundance (each component is shown with a dotted line and the solid line is the sum of all components). This model does not fit the data well either.

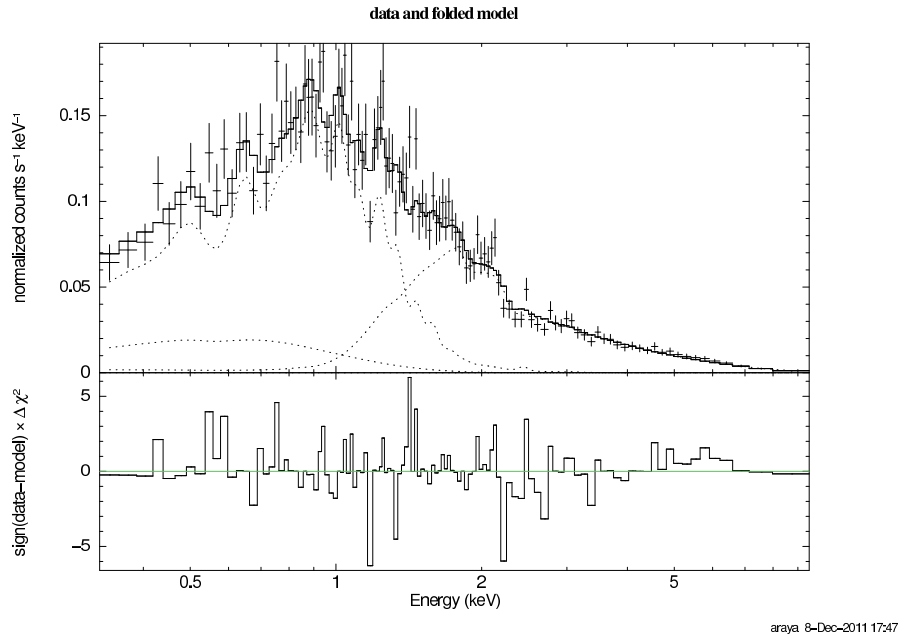


Fig. 5.— Same as Fig. 4, but with variable abundances. This is the best-fit model.

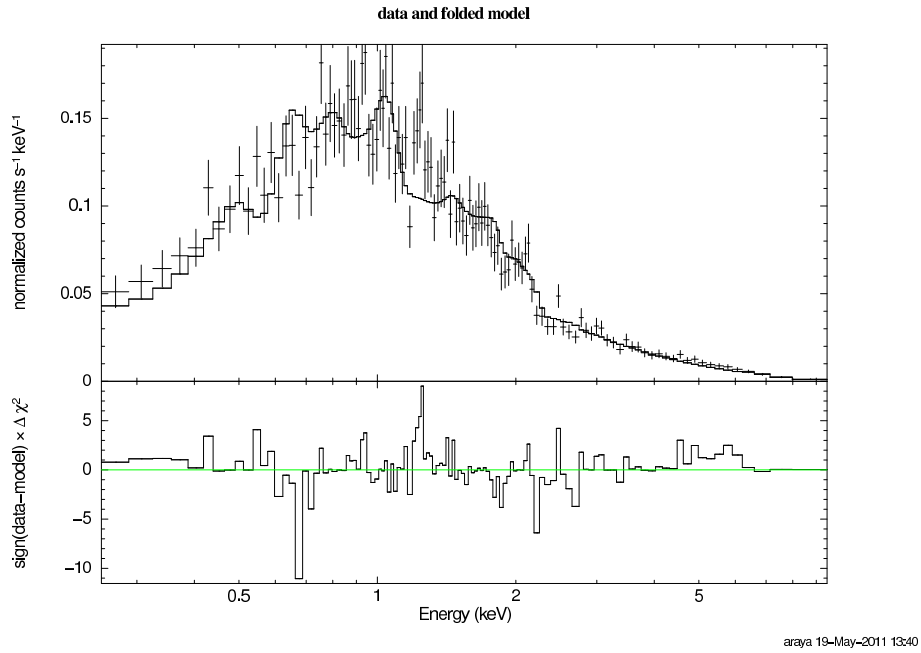


Fig. 6.— The spectrum fitted with an absorbed power-law plus an ionized reflection component. Contributions to χ^2 are presented in the bottom panel. This model does not provide a good fit.

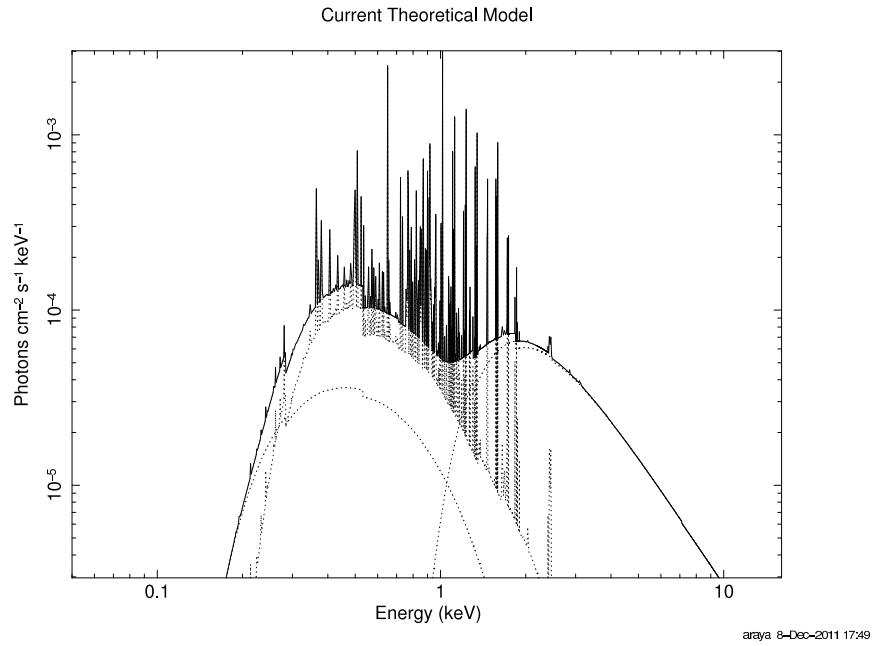


Fig. 7.— Theoretical model of the best fit spectrum showing the different components (absorbed power law, absorbed thermal plasma and black body).

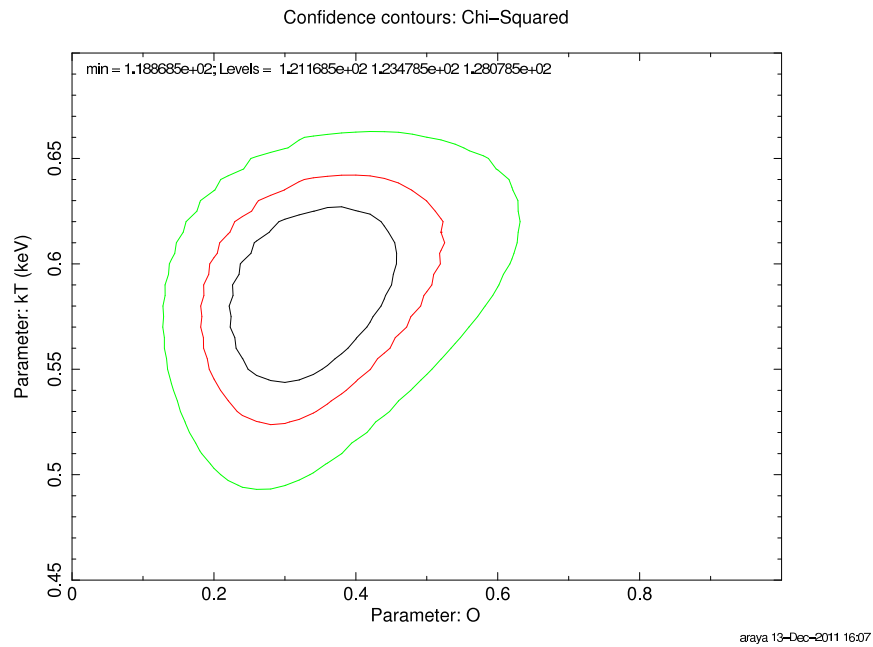


Fig. 8.— χ^2 contours for the abundance of oxygen and temperature of the plasma in the best fit model (Solar abundance is 1). Sub-solar oxygen abundance is clearly required.

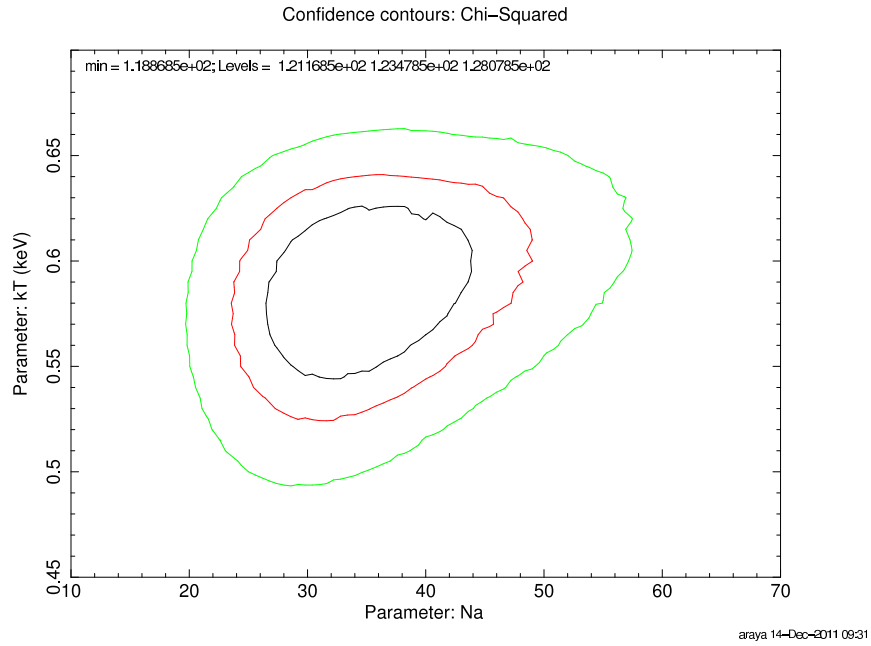


Fig. 9.— χ^2 contours for the abundance of sodium and temperature of the plasma in the best fit model (Solar abundance is 1). Sodium abundance appears to be super-solar.

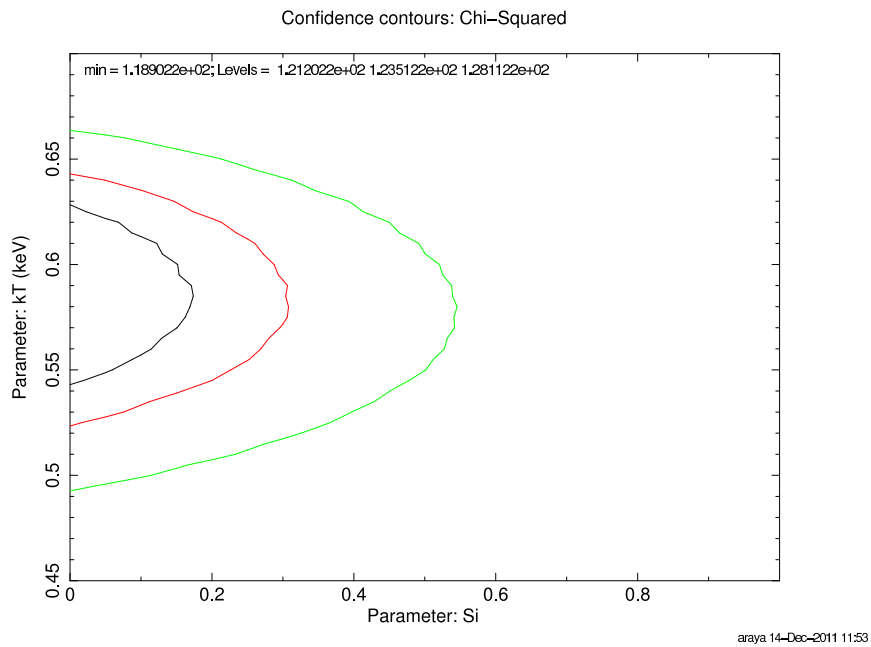


Fig. 10.— χ^2 contours for the abundance of silicon and temperature of the plasma in the best fit model (Solar abundance is 1). Sub-solar silicon is clearly indicated.

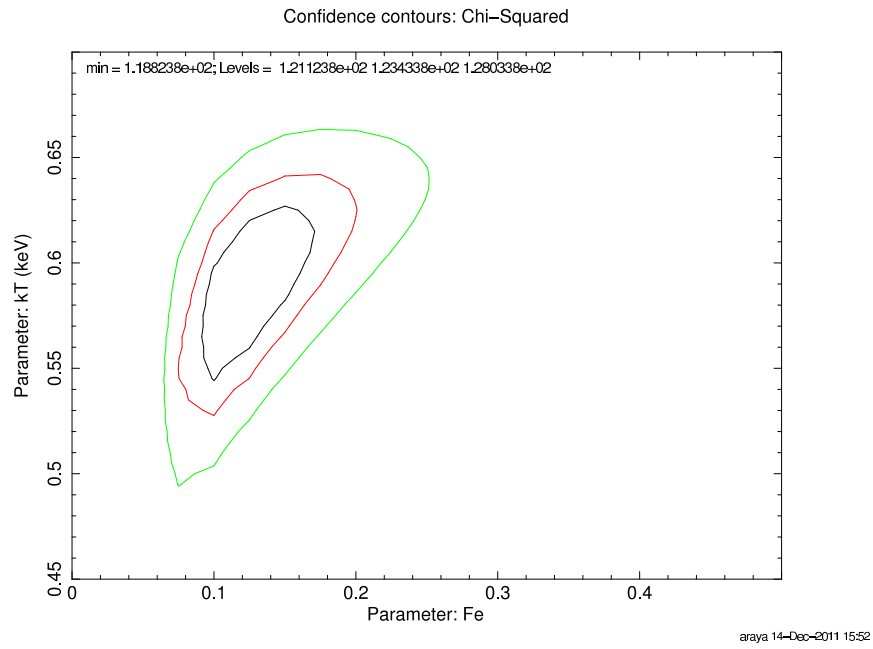


Fig. 11.— χ^2 contours for the abundance of iron and temperature of the plasma in the best fit model (Solar abundance is 1). Again, sub-solar iron abundance is required by the fit.

REFERENCES

- Adams, F. C., Graff, D. S., & Richstone, D. O. 2001, *ApJ*, 551, L31
- Baes, M., Buyle, P., Hau, G. K. T., & Dejonghe, H. 2003, *MNRAS*, 341, L44
- Begelman, M. C., Volonteri, M., & Rees, M. J. 2006, *MNRAS*, 370, 289
- Böker, T., Walcher, C. J., Rix, H. W., Häring, N., Schinnerer, E., Sarzi, M., van der Marel, R. P., Ho, L. C., Shields, J. C., Lisenfeld, U., & Laine, S. 2004, in *Astronomical Society of the Pacific Conference Series*, Vol. 322, *The Formation and Evolution of Massive Young Star Clusters*, ed. H. J. G. L. M. Lamers, L. J. Smith, & A. Nota, 39–+
- Brand, K., Dey, A., Brown, M. J. I., Watson, C. R., Jannuzi, B. T., Najita, J. R., Kochanek, C. S., Shields, J. C., Fazio, G. G., Forman, W. R., Green, P. J., Jones, C. J., Kenter, A. T., McNamara, B. R., Murray, S. S., Rieke, M., & Vikhlinin, A. 2005, *ApJ*, 626, 723
- Cisternas, M., Jahnke, K., Inskip, K. J., Kartaltepe, J., Koekemoer, A. M., Lisker, T., Robaina, A. R., Scodreggio, M., Sheth, K., Trump, J. R., Andrae, R., Miyaji, T., Lusso, E., Brusa, M., Capak, P., Cappelluti, N., Civano, F., Ilbert, O., Impey, C. D., Leauthaud, A., Lilly, S. J., Salvato, M., Scoville, N. Z., & Taniguchi, Y. 2011, *ApJ*, 726, 57
- Dahlem, M., Weaver, K. A., & Heckman, T. M. 1998, *ApJS*, 118, 401
- Desroches, L.-B., & Ho, L. C. 2009, *ApJ*, 690, 267
- Di Matteo, T., Croft, R. A. C., Springel, V., & Hernquist, L. 2003, *ApJ*, 593, 56
- Dudik, R. P., Satyapal, S., Gliozzi, M., & Sambruna, R. M. 2005, *ApJ*, 620, 113
- Ferrarese, L., & Ford, H. 2005, *Space Sci. Rev.*, 116, 523
- Ferrarese, L., & Merritt, D. 2000, *ApJ*, 539, L9
- Fields, D. L., Mathur, S., Krongold, Y., Williams, R., & Nicastro, F. 2007, *ApJ*, 666, 828
- Fields, D. L., Mathur, S., Pogge, R. W., Nicastro, F., Komossa, S., & Krongold, Y. 2005, *ApJ*, 634, 928
- Filippenko, A. V., & Sargent, W. L. W. 1989, *ApJ*, 342, L11

- Gebhardt, K., Bender, R., Bower, G., Dressler, A., Faber, S. M., Filippenko, A. V., Green, R., Grillmair, C., Ho, L. C., Kormendy, J., Lauer, T. R., Magorrian, J., Pinkney, J., Richstone, D., & Tremaine, S. 2000, *ApJ*, 539, L13
- Ghosh, H. 2009, PhD thesis, The Ohio State University
- Ghosh, H., Mathur, S., Fiore, F., & Ferrarese, L. 2008, *ApJ*, 687, 216
- . 2011, *ApJ*, submitted
- Governato, F., Brook, C., Mayer, L., Brooks, A., Rhee, G., Wadsley, J., Jonsson, P., Willman, B., Stinson, G., Quinn, T., & Madau, P. 2010, *Nature*, 463, 203
- Grier, C. J., Mathur, S., Ghosh, H., & Ferrarese, L. 2011, *ApJ*, 731, 60
- Guainazzi, M., Risaliti, G., Nucita, A., Wang, J., Bianchi, S., Soria, R., & Zezas, A. 2009, *A&A*, 505, 589
- Gültekin, K., Richstone, D. O., Gebhardt, K., Lauer, T. R., Tremaine, S., Aller, M. C., Bender, R., Dressler, A., Faber, S. M., Filippenko, A. V., Green, R., Ho, L. C., Kormendy, J., Magorrian, J., Pinkney, J., & Siopis, C. 2009, *ApJ*, 698, 198
- Hamann, F., & Ferland, G. 1999, *ARA&A*, 37, 487
- Hamann, F., & Simon, L. E. 2010, in *IAU Symposium*, Vol. 265, *IAU Symposium*, ed. K. Cunha, M. Spite, & B. Barbuy, 171–178
- Häring, N., & Rix, H.-W. 2004, *ApJ*, 604, L89
- Ho, L. C. 2008, *ARA&A*, 46, 475
- Hopkins, P. F., Hernquist, L., Cox, T. J., Di Matteo, T., Robertson, B., & Springel, V. 2006, *ApJS*, 163, 1
- Kennicutt, Jr., R. C., Armus, L., Bendo, G., Calzetti, D., Dale, D. A., Draine, B. T., Engelbracht, C. W., Gordon, K. D., Grauer, A. D., Helou, G., Hollenbach, D. J., Jarrett, T. H., Kewley, L. J., Leitherer, C., Li, A., Malhotra, S., Regan, M. W., Rieke, G. H., Rieke, M. J., Roussel, H., Smith, J.-D. T., Thornley, M. D., & Walter, F. 2003, *PASP*, 115, 928
- Kirhakos, S. D., & Steiner, J. E. 1990, *AJ*, 99, 1722
- Koopmann, R. A., Haynes, M. P., & Catinella, B. 2006, *AJ*, 131, 716

- Kormendy, J., & Bender, R. 2011, *Nature*, 469, 377
- Levenson, N. A., Weaver, K. A., & Heckman, T. M. 2001, *ApJ*, 550, 230
- Magorrian, J., Tremaine, S., Richstone, D., Bender, R., Bower, G., Dressler, A., Faber, S. M., Gebhardt, K., Green, R., Grillmair, C., Kormendy, J., & Lauer, T. 1998, *AJ*, 115, 2285
- Marconi, A., Risaliti, G., Gilli, R., Hunt, L. K., Maiolino, R., & Salvati, M. 2004, *MNRAS*, 351, 169
- Martini, P., Kelson, D. D., Mulchaey, J. S., & Trager, S. C. 2002, *ApJ*, 576, L109
- McAlpine, W., Satyapal, S., Gliozzi, M., Cheung, C. C., Sambruna, R. M., & Eracleous, M. 2011, *ApJ*, 728, 25
- McLure, R. J., & Dunlop, J. S. 2002, *MNRAS*, 331, 795
- Menci, N., Fiore, F., Perola, G. C., & Cavaliere, A. 2004, *ApJ*, 606, 58
- Merritt, D., & Ferrarese, L. 2001, *ApJ*, 547, 140
- Mullaney, J. R., Pannella, M., Daddi, E., Alexander, D. M., Elbaz, D., Hickox, R. C., Bournaud, F., Altieri, B., Aussel, H., Coia, D., Danmerbauer, H., Dasyra, K., Dickinson, M., Hwang, H. S., Kartaltepe, J., Leiton, R., Magdis, G., Magnelli, B., Popesso, P., Valtchanov, I., Bauer, F. E., Brandt, W. N., Del Moro, A., Hanish, D. J., Ivison, R. J., Juneau, S., Luo, B., Lutz, D., Sargent, M. T., Scott, D., & Xue, Y. Q. 2011, *MNRAS*, 1756
- Paturel, G., Theureau, G., Bottinelli, L., Gouguenheim, L., Coudreau-Durand, N., Hallet, N., & Petit, C. 2003, *A&A*, 412, 57
- Peterson, B. M., Bentz, M. C., Desroches, L.-B., Filippenko, A. V., Ho, L. C., Kaspi, S., Laor, A., Maoz, D., Moran, E. C., Pogge, R. W., & Quillen, A. C. 2005, *ApJ*, 632, 799
- Ptak, A., Serlemitsos, P., Yaqoob, T., & Mushotzky, R. 1999, *ApJS*, 120, 179
- Reines, A. E., Sivakoff, G. R., Johnson, K. E., & Brogan, C. L. 2011, *Nature*, 470, 66
- Satyapal, S., Böker, T., McAlpine, W., Gliozzi, M., Abel, N. P., & Heckman, T. 2009, *ApJ*, 704, 439
- Satyapal, S., Vega, D., Heckman, T., O’Halloran, B., & Dudik, R. 2007, *ApJ*, 663, L9

- Schawinski, K., Treister, E., Urry, C. M., Cardamone, C. N., Simmons, B., & Yi, S. K. 2011, *ApJ*, 727, L31
- Seth, A., Agüeros, M., Lee, D., & Basu-Zych, A. 2008, *ApJ*, 678, 116
- Shankar, F., Salucci, P., Granato, G. L., De Zotti, G., & Danese, L. 2004, *MNRAS*, 354, 1020
- Shields, J. C., Walcher, C. J., Böker, T., Ho, L. C., Rix, H.-W., & van der Marel, R. P. 2008, *ApJ*, 682, 104
- Vasudevan, R. V., & Fabian, A. C. 2007, *MNRAS*, 381, 1235
- Volonteri, M., & Natarajan, P., 2009, *MNRAS*, 400, 1911
- Volonteri, M., Natarajan, P., & Gültekin, K. 2011, *ApJ*, 737, 50
- Woo, J.-H., & Urry, C. M. 2002, *ApJ*, 579, 530
- Zhang, W. M., Soria, R., Zhang, S. N., Swartz, D. A., & Liu, J. F. 2009, *ApJ*, 699, 281

Table 1. Spectral Models

Model ID	Model	Component	Parameters* **	χ^2_ν (dof)
1	absorbed power-law and thermal plasma with solar abundance	power-law mekal	$N_H = 1.02 \pm 0.05$ $N_H = 0.86 \pm 0.05, kT = 0.11 \pm 0.01$	2.35 (112)
2	absorbed power-law and thermal plasma with non-solar abundance	power-law mekal	$N_H = 1.06 \pm 0.05$ $N_H = 0.82 \pm 0.05, kT = 0.12 \pm 0.01, \text{abund} = 0.3 \pm 0.3$	2.27 (111)
3	absorbed power-law and reflection	power-law reflionx	$N_H = 1.6 \pm 0.2$ $N_H = 0.23^{+0.03}_{-0.02}, \text{Fe/solar} = 4.5^{+1.3}_{-2.5}, X_i = 1300^{+700}_{-600}$	1.39 (113)
4	absorbed power-law and vmekal with solar abundance	power-law vmekal	$N_H = 1.39 \pm 0.06$ $N_H = 0.0^{+0.03}, kT = 0.70 \pm 0.01$	2.35 (112)
5	absorbed power-law and vmekal with non-solar abundance	power-law vmekal	$N_H = 1.9^{+0.1}_{-0.2}$ $N_H = 0.07^{+0.02}_{-0.03}, kT = 0.59^{+0.04}_{-0.05}$ $O = 0.33^{+0.14}_{-0.12}, \text{Na} = 34^{+11}_{-8}$ $\text{Si} = 0^{+0.2}_{-0}, \text{Fe} = 0.12^{+0.06}_{-0.04}, \text{Ni} = 0^{+0.4}_{-0}$	1.11 (107)

*In all the models: Galactic absorption was added with $N_H = 2.11 \times 10^{20} \text{ cm}^{-2}$ and the photon index of the power-law is $\Gamma = 2.46$ (obtained fitting only for $E \geq 2.5 \text{ keV}$). These two parameters were always frozen when fitting. All the models also have a blackbody with $kT=0.2 \text{ keV}$ and flux $F(0.2-10 \text{ keV})=2.5 \times 10^{-14}$ accounting for the source B.

**Al column densities are in units of 10^{22} cm^{-2} , temperatures in keV.